In vivo cross-linking and transmembrane helix dynamics support a non-piston model of signaling within *E. coli* EnvZ

Rahmi Yusuf[a,1], Tuyết Linh Nguyễn[a,1], Annika Heininger[b], Robert J. Lawrence[a], Benjamin A. Hall[c*] and Roger R. Draheim[a,d*]

[a]School of Pharmacy and Biomedical Sciences, University of Portsmouth, Portsmouth, PO1 2DT, England, UK; [b]Institute of Biochemistry, Biocenter, Goethe University Frankfurt, D-60438 Frankfurt, Germany; [c]MRC Cancer Unit, University of Cambridge, Cambridge, CB2 0XZ, England, UK; [d]Institute of Biological and Biomedical Science, University of Portsmouth, Portsmouth, PO1 2DT, England, UK

Running title: Non-piston transmembrane communication by EnvZ

[1]These authors contributed equally

*To whom correspondence should be addressed (B. A. H. or R. R. D.):

MRC Cancer Unit
University of Cambridge
Hutchison / MRC Research Centre
Box 197, Cambridge Medical Campus
Cambridge
CB2 0XZ
United Kingdom
tel: + 44 (0) 1223 763240
fax: + 44 (0) 1223 763241

University of Portsmouth
School of Pharmacy and Biomedical Sciences
St. Michael's Building
White Swan Road
Portsmouth
PO1 2DT
United Kingdom
tel: +44 (0)23 9284 2133
fax: +44 (0)23 9284 3565

Keywords

porin balance / transmembrane communication / coarse-grained molecular dynamics / sulfhydryl-reactivity / transmembrane helix dynamics

55 In gram-negative bacteria, porins span the outer membrane and control the influx of several
56 prominent groups of antibiotics[1,2]. Thus, it should not be surprising that expression of these porins
57 is often altered in clinical isolates that exhibit multidrug resistance (MDR)[3-9]. The major regulator
58 of porin expression in *Escherichia coli* is EnvZ, a canonical sensor histidine kinase (SHK). It
59 allosterically processes periplasmic interactions with MzrA and cytoplasmic osmosensing into a
60 single unified change in the ratio of its kinase and phosphatase activities[10-15]. Unfortunately, the role
61 of the transmembrane domain (TMD) in communicating these signals across the cellular membrane
62 remains not well understood. Here, we employed *in vivo* sulfhydryl-reactivity to probe the
63 dynamics of individual TM2 helices within the TMD and demonstrate that upon stimulus
64 perception, EnvZ employs a non-piston-type mechanism of transmembrane communication. *In*
65 *silico* coarse-grained molecular dynamics (CG-MD) simulations with EnvZ TM2 are in agreement
66 with these *in vivo* results. We conclude by discussing these results within the context of allosteric
67 processing by EnvZ and propose that these results can be used to predict and classify
68 transmembrane communication by various SHKs.
69
70 Most porins involved in antibiotic transport by gram-negative bacteria belong to the classical OmpF
71 and OmpC families[2]. Transcription of these porins is governed by the intracellular concentration of
72 phospho-OmpR (OmpR-P), which is controlled by EnvZ in response to changes in periplasmic
73 interactions with MzrA and environmental osmolarity[10-15] (Figure S1A). At low intracellular levels
74 of OmpR-P, transcription of *ompF* is upregulated, whereas at higher levels of OmpR-P,
75 transcription of *ompF* is repressed and transcription of *ompC* is activated. This results in a
76 predominance of OmpF at low osmolarity and OmpC at higher osmolarities or in the presence of
77 MzrA (Figure S1B)[16-18]. Dramatic modification of porin balance, which has been observed within
78 clinical isolates from patients undergoing antibiotic treatment, strongly suggests that the underlying
79 mechanisms of porin regulation by EnvZ require further characterisation[3-9].

80

81 Comparison of recently published *apo* and *holo* high-resolution (~1.9 Å) crystal structures of the *E.*
82 *coli* nitrate sensor NarQ that contain the periplasmic, TM and HAMP domains reveal extensive
83 structural rearrangements involving a piston-like motion of TM1 relative to TM2 of approximately
84 2.5 Å. These displacements result in a lever-like rotation of individual HAMP domains upon
85 binding of cognate ligand[19]. Based on these results, the authors posit that receptors containing a
86 membrane-adjacent HAMP domain function by a piston-type displacement of TM helices while
87 those that lack such domains transduce signal by rotation of TM helices. We previously postulated a
88 related yet different categorisation of signalling mechanisms also based on the domain structure of
89 bacterial receptors[20]. We proposed that receptors containing a periplasmic four-helix bundle
90 transduce signal across the membrane by piston-type displacements and that the attached
91 membrane-adjacent HAMP domains might possess one of a multitude of signalling mechanisms
92 including a gearbox-type rotation[21], a dynamic bundle[22] or potentially other mechanisms[20].
93 Differentiating between these classification systems will provide a theoretical framework for
94 understanding domain-based intra-protein allosteric communication by bacterial receptors.

95

96 Here, we have analysed transmembrane signalling within EnvZ for several reasons. Firstly, because
97 of its aforementioned importance in regulating bacterial porin expression. Understanding how EnvZ
98 transduces signal would be a significant step toward direct manipulation of porin balance in
99 bacterial cells exhibiting MDR. Secondly, it examines whether SHKs that possess membrane-
100 adjacent HAMP domains function solely by piston-type displacements or whether other signalling
101 mechanisms might be employed. The results here with EnvZ are compared with previous findings
102 from the aspartate chemoreceptor (Tar) and the recent NarQ structures[19,23-25]. These three are ideal
103 candidates for comparison because they all possess a membrane-adjacent HAMP domain, however,

while Tar and NarQ possess a periplasmic four-helix bundle, EnvZ possesses a periplasmic PDC/CACHE domain[26,27].

Mapping TM2 surfaces important for EnvZ signal output

We previously created a Cys-less version of EnvZ from *E. coli* that had its sole Cys residue changed to an Ala residue (C277A). The Cys-less variant is expressed from pRD400, which results in the addition of a seven-residue linker (GGSSAAG) and a C-terminal V5 epitope (GKPIPNPLLGLDST). We previously found that the Cys-less version of EnvZ had similar steady-state signal output and response to environmental osmolarity as the wild-type version of EnvZ making it suitable for comparisons of *in vivo* sulfhydryl-reactivity and signal output analysis. We initially determined that no major rearrangements occur along the TM1-TM1' interface upon stimulus perception[28]. As minimal change was observed along this helical interface in response to osmolarity, we continued by examining the TM2-TM2' interface. We began by determining which residues comprise TM2 by subjecting the full EnvZ sequence to DGpred[29] and TMHMM v2.0[30], which suggested that Leu-160 to Ile-181 and Leu-160 to Ile-179 comprise TM2 respectively. Based on these analyses, we employed site-directed mutagenesis using the Cys-less variant as a template to create a library of single-Cys-containing EnvZ proteins that spanned from positions 156 to 184 (Figure 1). We observed that nearly the entire library was expressed within EPB30/pRD400 cells grown under the low- or high-osmolarity regime. Variants possessing a Cys at position 156 showed low levels of expression when grown under the low-osmolarity (0% sucrose) regime. However, when grown under the high-osmolarity regime, no variants showed reduced expression level (Figure S2). These results indicate that the library is suitable for further *in vivo* experimentation.

We began by expressing each of the single-Cys-containing variants in EPB30/pRD400 cells, which

129 allowed us to measure CFP fluorescence, YFP fluorescence, and to calculate the CFP/YFP ratio that
130 estimates steady-state EnvZ signal output (Figure S1B). Cells expressing the Cys-less C277A were
131 used as a baseline comparison (Figure S3). When EPB30/pRD400 cells are grown under the low-
132 osmolarity regime, a shift in signalling output toward the "on" or kinase-dominant state results in
133 increased CFP fluorescence, reduced YFP fluorescence and an increase in the overall CFP/YFP
134 ratio, while a shift toward the "off" or phosphatase-dominant state appears as decreased CFP,
135 increased YFP and a decrease in CFP/YFP ratio (Figures 2 and S4).
136
137 Several trends were observed during analysis of the library of Cys-containing EnvZ receptors.
138 When EPB30/pRD400 cells were grown under the low-osmolarity regime, EnvZ was less tolerant
139 of Cys substitutions at the N- and C-terminal regions of the library. At the N-terminus, signal output
140 from receptors containing a Cys at positions 156, 162 and 163 were very elevated, exhibiting
141 greater than a 5-fold increase in CFP/YFP, while receptors possessing a Cys in the C-terminus at
142 positions 179, 181, 182 and 184 were elevated, possessing over a 2-fold increase in CFP/YFP.
143 These boundary regions appear to flank a core of alternating increases and decreases in EnvZ signal
144 output, as observed between residue positions 165 and 180, suggesting that multiple tightly packed
145 EnvZ helices exist within the hydrophobic core of the inner membrane (Figures 2A and 2B). When
146 grown under the high-osmolarity regime, a pattern appeared where Cys substitutions resulted in
147 significant decreases in signal output (Figure 2C). Of the 29 mutants analysed, 13 supported less
148 than 75% of the normal wild-type signal output.
149
150 Perhaps most striking is the inverse effect on EnvZ signal output of the Cys substitutions that flank
151 the hydrophobic core of TM2. For these residues, when grown under the low-osmolarity regime, the
152 presence of a Cys residue resulted in an increase in signal output of more than 25%, i.e. shifted
153 toward the on or kinase-dominant state (red dots in Figure 2A) and a reduction in signal output of

154 more than 25%, i.e. shifted toward the off or phosphate-dominant state, when grown under the high-
155 osmolarity regime (blue dots in Figure 2C). These flipped positions reside at the N- and C-terminal
156 ends of the region we examined and outside of the proposed hydrophobic TMD core (Figure 2).
157 Within the hydrophobic core, Cys substitutions show similar changes when cells are grown under
158 the low- and high-osmolality regimes. These results suggest that the flanking regions are not simply
159 rigid structural conduits for signal transduction but may have higher-order roles in signal
160 transduction, such as MzrA interaction or functioning as a control cable at the N- and C-terminal
161 regions respectively[14,15,22].

162

163 *Identifying surfaces involved in TM2-TM2' interactions*

164

165 Sulfhydryl-reactivity experimentation is well-characterised and has been employed on many soluble
166 and membrane-spanning proteins and higher-order complexes[31]. The *in vivo* nature of this assay
167 facilitated mapping of the TM2-TM2' interface under different osmotic conditions, which is an
168 important first step toward understanding how EnvZ processes allosteric inputs from periplasmic
169 MzrA binding and cytoplasmic osmosensing into a single uniform modulation of bacterial porin
170 balance (Figures 1 and S1). In a similar manner to mapping TM1-TM1' interactions[28], Cys-
171 containing EnvZ variants were expressed in EPB30/pRD400 cells and upon entering the early
172 exponential phase ($OD_{600nm} \approx 0.25$) they were subjected to 250 μM molecular iodine for 10 minutes
173 analysed by non-reducing SDS-PAGE and immunoblotting (Figure S5).

174

175 We observed three distinct regions within TM2. The N-terminal region (region I in Figure 3),
176 comprised of residues 156 to 163, exhibited significant cross-linking under the low-osmolarity
177 regime (0% sucrose) and almost no crosslinking under the high-osmolarity (15% sucrose) regime.
178 The second region (II) consisting of positions 164 to 179, demonstrated altering low and high levels

179 of disulphide-formation consistent the crossing of TM2 and TM2' within the hydrophobic core of
180 the TMD. The final region (III), from residues 180 to 184, shows no crosslinking (Figure 3). It
181 should be noted that this significant difference at the periplasmic end of the TMD between cells
182 grown under the low- and high-osmolarity regime was not observed during similar analyses of
183 TM1[28].
184
185 *Molecular simulations of the wild-type and aromatically tuned variants of EnvZ TM2*
186
187 The piston-type model of transmembrane communication is founded upon the central tenant that the
188 vertical position of TM2 relative to the lipid bilayer changes upon stimulus perception. Previous
189 work with TM2 of Tar demonstrates that repositioning the aromatic residues at the cytoplasmic end
190 of TM2, known as aromatic tuning[32], repositions the helix within a biological membrane[33] and that
191 this repositioning causes an incremental change in signal output[32]. These results served as an
192 experimental framework to optimise SIDEKICK software capable of high-throughput parallelised
193 coarse-grained molecular dynamics (CG-MD) simulations, which demonstrated that aromatic
194 tuning repositioned the TM2 helix *in silico* in a manner consistent with both the *in vivo* results and a
195 piston-type mechanism of transmembrane communication[34].
196
197 Based on these extensive results and the recent suggestion that mechanisms employed by SHKs
198 during TM communication correlate with the presence of a membrane-adjacent HAMP domain, we
199 performed analogous *in silico* experimentation with EnvZ, which possesses a membrane-adjacent
200 HAMP domain but substitutes a periplasmic PDC/CACHE domain for the four-helix bundle present
201 in Tar and NarQ[19,26,27,35]. We previously performed aromatic tuning with TM2 of EnvZ and found
202 that signal output was not correlated with the absolute vertical position of the aromatic residues as

203 was shown for Tar TM2, which suggested that EnvZ does not transduce signal output across the
204 membrane by a piston-type displacement[36].
205
206 To interpret the results of our GC-MD analysis, we categorised the signal output of these
207 aromatically tuned EnvZ variants[36]. For several two-component signalling circuits, including the
208 EnvZ/OmpR, PhoQ/PhoP and CpxA/CpxR circuits, the steady-state output of the signalling circuits
209 has been shown to be independent of the level of SHK present[36-39]. However, in circuits containing
210 the tuned variants of EnvZ, a different relationship between steady-state signal output and receptor
211 level was observed, suggesting that the ratio of kinase to phosphatase activities was different within
212 each receptor and always different than wild-type EnvZ[36]. Based on this analysis, we found that the
213 WLF-1 variant possessed the highest signal output while the WLF-5, WLF-4 and WLF-3 variants
214 possessed only slightly higher activity than wild-type EnvZ, which maintained receptor-
215 concentration dependent robustness unlike the tuned variants. WLF-2 and WLF+1 were found to
216 possess reduced signal output, while WLF+2 possessed the lowest overall signal output. These
217 differences were previously quantified by analysing the slope of the change in CFP/YFP against the
218 amount of receptor present and are visually represented in Figure S6[36]. These classifications are
219 employed during interpretation of the CG-MD results in Figure 4.
220
221 Based on these previous results and the absence of asymmetric TM2 displacement observed within
222 the *in vivo* sulfhydryl-reactivity assay (Figure 3), we assessed whether molecular simulations would
223 lend credibility to a non-piston type of transmembrane communication employed by EnvZ. We
224 began by designing tuned TM2 sequences to subject to GC-MD simulations that matched those
225 previously used during the aromatic tuning experimentation (Figure 4A). Unlike analogous
226 experimentation with TM2 of Tar, no trend in helix displacement was observed (Figure 4B, Table

227 S1). This indicates that the mutations do not in isolation move the helix up and down in the
228 membrane and would appear to rule out a pure piston motion as previously observed in Tar[34].
229
230 An alternative mechanism for signal transduction is to induce a tilt in the helix relative to the
231 bilayer normal. This was originally proposed in Tar on the basis of crystallographic analysis of the
232 receptor domain[40], and led to the proposal of a "swinging piston" where both displacement and tilt
233 contributed to signal transduction. In addition, this would be consistent with a scissor-type model of
234 TM communication proposed to be utilised by PhoQ[41,42], which possesses a periplasmic
235 PDC/CACHE domain[43]. In testing the tuned EnvZ TM2 helices, a change in the extent of tilting
236 was observed during the CG-MD simulations (Figure 4C, Table S2). It was found that a reduction
237 in tilt, to a mean tilt of between 22 and 24 degrees, compared to the wild-type TM2 sequence with a
238 tilt of approximately 26 degrees correlated with a decreased signal output (phosphatase-biased, dark
239 blue). Interestingly, an increase in tilt to more than 29 degrees correlated with extremely biased
240 signal output, *i.e.* highly kinase-dominant (WLF-1, pink) and highly phosphatase-dominant
241 (WLF+2, bright blue). Taken together, these results demonstrate that tilt, rather than vertical
242 displacement, does correlate with altered signal output from EnvZ.
243
244 Finally, a rotational/gearbox model of TMD-HAMP communication has also been proposed for
245 EnvZ[21,44]. Central to this model is that interconversion between the kinase-dominant and
246 phosphatase-dominant signalling states can be accomplished by rotation of the individual HAMP
247 helices in unison by 26 degrees. Within our simulations, we observed some consistency with the
248 gearbox model of HAMP signalling, especially when the WLF-1 helix possessed a mean azimuthal
249 rotation that is 25 degrees different than wild-type EnvZ (pink in Figure 4D). The full-length WLF-
250 1 receptor was determined to the most highly kinase-biased tuned receptor we studied. The TM
251 helix from the most phosphatase-biased receptor (WLF+2) possessed a mean azimuthal rotation of

252 an additional 15 degrees. For the simulations involving other helices, it was not possible to
253 differentiate them into separate classes.
254
255 Here, our *in vivo* analysis demonstrated that only the periplasmic end of EnvZ TM2 undergoes a
256 conformational transition upon stimulus perception suggesting that the asymmetric piston-type
257 displacement employed by Tar is not used by EnvZ. Previously, a linear correlation was observed
258 between the position of the aromatic residue in Tar TM2, the position of the helices *in vitro* and *in*
259 *silico* and the signal output from each Tar receptor[32,33,45]. Here, *in silico* analysis of EnvZ TM2
260 demonstrates that such a linear correlation is absent suggesting that EnvZ functions by a non-piston
261 mechanism in which both tilting and azimuthal rotation play a substantial role in modulation of
262 signal output (Figure 4).
263
264 *Correlations between domain composition and mechanisms of signal transduction*
265
266 The authors of the recent NarQ structures posit that the presence or absence of the membrane-
267 adjacent HAMP domain may be the difference between receptors employing piston-type
268 mechanisms of transmembrane communication as compared to other signalling mechanisms[19].
269 However, differences employed during transmembrane communication by the Tar and EnvZ TMDs
270 observed here and previously strongly suggest that Tar and EnvZ possess different mechanism of
271 TM communication. Our previous work analysed AS1 helices from *E. coli* NarX, *E. coli* Tar, *E.*
272 *coli* EnvZ and Af1503, the HAMP domain resulting in the initial high-resolution structure[21], and
273 found that the Tar and NarX AS1 helices possess similar properties, which AS1 helices from both
274 EnvZ and Af1503 lack. Recent comparisons of the *apo* and ligand-bound structures of the
275 combined periplasmic-TM-HAMP domain from *E. coli* NarQ demonstrate that binding of ligand
276 results in symmetrical displacements of TM1 relative to TM2 of approximately 2.5 Å.[19] These

277 results are similar to Tar, which functions by asymmetrical TM2 displacement also possesses a
278 periplasmic four-helix-bundle[23-25,35]. Thus, we conclude that *E. coli* EnvZ functions by a non-piston
279 mechanism of transmembrane communication that is different than Tar, NarX and NarQ, which
280 communicate across the membrane by piston-type displacements. Furthermore, we propose that the
281 TM signalling mechanisms can be predicted and assigned based upon the domain(s) present in the
282 periplasmic region of a bacterial TM-spanning receptor.
283
284 **Methods**
285
286 *Bacterial strains and plasmids*
287
288 *E. coli* strains DH10B (New England Biolabs) or MC1061[46] were used for DNA manipulations,
289 while strain K-12 MG1655[47] served a non-fluorescent strain that was used to control for light
290 scattering and cellular autofluorescence. *E. coli* strains MDG147 [MG1655 Φ(*ompF*$^+$-*yfp*$^+$)
291 Φ(*ompC*$^+$-*cfp*$^+$)] [48] and EPB30 (MDG147 *envZ::kan*)[39] were employed for analysis of EnvZ signal
292 output. Plasmid pRD400[36] retains the IPTG-based induction of EnvZ from plasmid pEnvZ[49] while
293 adding a seven-residue linker (GGSSAAG)[50] and a C-terminal V5 epitope tag
294 (GKPIPNPLLGLDST)[51]. Plasmid pEB5[37] was employed as an empty control vector.
295
296 *Selection of residues comprising TM2 of EnvZ*
297
298 The primary sequence of EnvZ from *E. coli* K-12 MG1655 was subjected to DGpred using a
299 minimal window of 9 residues and a maximal window of 40 residues[29]. Alternatively, a software
300 package that identifies TM helices with a Markov model (TMHMM v2.0)[30] was also employed.
301 These software packages suggested that Leu-160 to Ile-181 and Leu-160 to Ile-179 comprise TM2

302 respectively. Based on these results and to maximize the probability of including all residues within
303 TM2, we targeted all residues between positions 156 to 184 for the creation of a library of single-
304 Cys-containing EnvZ receptors.
305
306 *Analysis of EnvZ signal output* in vivo
307
308 Bacterial cultures were grown as described previously[36] with minor modification. MDG147 or
309 EPB30 cells were transformed with pRD400 expressing one of the single-Cys-containing EnvZ
310 receptors or pEB5 (empty). Fresh colonies were used to inoculate 2-ml overnight cultures of
311 minimal medium A[52] supplemented with 0.2% glucose. Ampicillin, sucrose and IPTG were added
312 as appropriate. Cells were grown overnight at 37 °C and diluted at least 1:1000 into 7 ml of fresh
313 medium. Upon reaching an $OD_{600nm} \approx 0.3$, chloramphenicol was added to a final concentration of
314 170 μg/ml. Fluorescent analysis was immediately conducted with 2 ml of culture and a Varian Cary
315 Eclipse (Palo Alto, CA). CFP fluorescence was measured using an excitation wavelength of 434 nm
316 and an emission wavelength of 477 nm, while YFP fluorescence was measured using an excitation
317 wavelength of 505 nm and an emission wavelength of 527 nm. These values were corrected for cell
318 density and for light scattering/cellular autofluorescence by subtracting the CFP and YFP
319 fluorescence intensities determined for MG1655/pEB5 cells.
320
321 *Analysis of sulfhydryl-reactivity* in vivo
322
323 Cells were grown as described above with minor chnges. Upon reaching an $OD_{600nm} \sim 0.3$, cells
324 were subjected to between 250 μM molecular iodine for 10 min while incubating at 37 °C. The
325 reaction was terminated with 8 mM N-ethylmaleimide (NEM) and 10 mM EDTA. Cells were
326 harvested by centrifugation and resuspended in standard 6X non-reducing SDS-PAGE buffer

327 supplemented with 12.5 mM NEM. Cell pellets were analysed on 10% SDS/acrylamide gels.
328 Standard buffers and conditions were used for electrophoresis, immunoblotting and detection with
329 enhanced chemiluminescence[53]. Anti-V5 (Invitrogen) was the primary antibody and peroxidase-
330 conjugated anti-mouse IgG (Sigma) was the secondary antibody. Digitized images were acquired
331 with a ChemiDoc MP workstation (Bio-RAD), analysed with ImageJ v1.49[54] and quantified with
332 QtiPlot v0.9.8.10.
333
334 *CG-MD simulations with SIDEKICK*
335
336 As previously described[34], coarse-grained molecular dynamics (CG-MD) simulations were
337 performed using the MARTINI forcefield with an approximately 4:1 mapping of non-H atoms to
338 CG particles. Lennard-Jones interactions between 4 classes of particles: polar (P), charged (Q),
339 mixed polar/apolar (N) and hydrophobic apolar (C) were used to treat interparticle interactions.
340 Within MARTINI, P and C particle types were subdivided to reflect varying degrees of polarity.
341 Short range electrostatic interactions were treated Coulombically, shifted to zero between 0 and 12
342 Å. Lennard-Jones interactions were shifted to zero between 9 and 12 Å. α-helix integrity was
343 maintained via dihedral restraints. Peptide termini were treated as uncharged. Simulations were
344 performed using Gromacs 3[55]. Temperature was coupled using a Berendsen thermostat at 323 K
345 (τ_T=1 ps), and pressure was coupled semi-isotropically (across XY/Z) at 1 bar
346 (compressibility=3×10^{-5} bar^{-1}, τ_P=10 ps). The initial simulation timestep was 20 fs. Initial models
347 of the TM α-helices were generated as ideal, atomistically detailed α-helices using standard
348 backbone angles and side- chain conformers. These were then converted to coarse-grained as
349 described previously[34]. Around 128 DPPC molecules were used in each simulation along with
350 around 3000 CG water particles, giving a final system size of ~65×65×13 Å.
351

352 **Author contributions**

353

354 R. Y., T. L. N, B. A. H. and R. R. D. conceived and designed the experiments. R. Y., T. L. N., A. H.
355 and R. J. L. performed the experiments. R. Y., A. H., T. L. N., R. J. L., B. A. H. and R. R. D.
356 analysed the data. R. Y., T. L. N., B. A. H. and R. R. D. wrote the manuscript. All authors read and
357 approved the final manuscript.

358

359 **Acknowledgments**

360

361 R. Y. was generously supported by the Indonesia Endowment Fund for Education, Ministry of
362 Finance (S-4833/LPDP.3/2015). T. L. N. was supported by a grant from the Erasmus+ programme.
363 R. R. D. was supported with start-up funding from the Faculty of Science and from the Institute of
364 Biological and Biomedical Science (IBBS) at the University of Portsmouth. B. A. H. was
365 generously supported by the Royal Society (UF130039 to B. A. H.).

366

367 **Competing interests**

368

369 The authors declare no competing financial interests.

370

371 **Figure legends**

372

373 Figure 1. EnvZ functions as a homodimer with a cytoplasmic N-terminus, the first transmembrane
374 helix (TM1, white), a large periplasmic domain (sensor, white), the second transmembrane helix
375 (TM2, red), a membrane-adjacent HAMP domain (grey) and the cytoplasmic domains responsible
376 for dimerization and histidylphosphortransfer (DHp, black) and catalytic ATPase activity (CA,

377 black). The position of the original Cys-277 residue that was mutated to Ala to produce the Cys-less
378 EnvZ is provided. The residues subjected to Cys substitution and their position in the primary
379 sequence is provided. Signal output from each single-Cys-containing variant is compared to the
380 Cys-less (C277A) variant: less than 50% of Cys-less (light blue), between 50% and 75% of Cys-
381 less (dark blue), between 75% and 125% of Cys-less (grey), between 125% and 200% (dark red)
382 and greater than 200% (light red). Residue positions exhibited flipped signal output are indicated
383 with a plus. The extent of sulphydryl-reactivity is also presented in five categories based on dimer-
384 to-monomer ratio: no dimer present (white), less than 0.05 (light grey), between 0.05 and 0.2
385 (medium grey), between 0.2 and 0.5 (dark grey) and greater than 0.5 (red). Positions that exhibit a
386 significant change in cross-linking between the low- and high-osmolarity regimes are indicated with
387 a plus.
388
389 Figure 2. Signal output from the library of single-Cys EnvZ variants. (A) CFP/YFP from
390 EPB30/pRD400 cells expressing one of single-Cys variants grown under the low-osmolarity (0%
391 sucrose) regime. On the right axis, these CFP/YFP ratios are compared to the Cys-less (C277A)
392 variant. (B) Magnified version of panel A in order to emphasise the region up to a 2-fold increase in
393 CFP/YFP. (C) CFP/YFP from EPB30/pRD400 cells expressing one of the single-Cys variants
394 grown under the high-osmolarity (15% sucrose) regime. On the right axis, these CFP/YFP ratios are
395 compared to the Cys-less (C277A) variant. The flipped mutants are highlighted with a red dot in
396 panel A (increased signal output) and a blue dot in panel C (decreased signal output). The shaded
397 areas represent the mean signal output from the Cys-less variant of EnvZ with a range of one
398 standard error of mean. These values are provided to aid in comparison. Error bars represent
399 standard deviation of the mean with a sample size of $n \geq 3$.

400 Figure 3. Extent of sulfhydryl-reactivity for each single-Cys-containing EnvZ variant.
401 EPB30/pRD400 cells were grown under the low- (empty circles, 0% sucrose) or high-osmolarity

402 (filled circles, 15% sucrose) regimes and subjected to 250 μM molecular iodine for 10 minutes
403 when their OD_{600nm} reached approximately 0.25. As shown in Figure S5, this allowed us to
404 determine the dimer/monomer ratio represented on the Y-axis. Three distinct regions, denoted I, II
405 and III were observed and are described in the text. Error bars represent the standard error of the
406 mean with a sample size of $n \geq 3$.
407
408 Figure 4. Aromatic tuning and signal output from EnvZ. (A) When aromatic tuning was performed
409 in EnvZ, a Trp-Leu-Phe triplet (red) was repositioned within the C-terminal region of TM2. (B)
410 Helix displacements, (C) tilt distributions and (D) azimuthal rotational distributions of the
411 aromatically tuned EnvZ TM2 helices. Histograms are shown for all time points of all membranes
412 of each ensemble. Aromatically tuned mutants have been classified based on their signal output into
413 five categories: highly kinase biased (WLF-1; pink), moderately kinase biased (WLF-5, WLF-4,
414 WLF-3; red), balanced (wild-type; black), moderately phosphatase biased (WLF-2, WLF+1, dark
415 blue) and highly phosphatase biased (WLF+2, light blue).
416
417 **References**
418

419 1 Delcour, A. H. Solute uptake through general porins. *Frontiers in bioscience : a journal and*
420 *virtual library* **8**, d1055-1071, (2003).
421 2 Nikaido, H. Molecular basis of bacterial outer membrane permeability revisited.
422 *Microbiology and molecular biology reviews : MMBR* **67**, 593-656, (2003).
423 3 Elliott, E. *et al.* In vivo development of ertapenem resistance in a patient with pneumonia
424 caused by Klebsiella pneumoniae with an extended-spectrum beta-lactamase. *Clinical*
425 *infectious diseases : an official publication of the Infectious Diseases Society of America* **42**,
426 e95-98, (2006).
427 4 Hernandez-Alles, S. *et al.* Relationship between outer membrane alterations and
428 susceptibility to antimicrobial agents in isogenic strains of Klebsiella pneumoniae. *The*
429 *Journal of antimicrobial chemotherapy* **46**, 273-277, (2000).
430 5 Jacoby, G. A., Mills, D. M. & Chow, N. Role of beta-lactamases and porins in resistance to
431 ertapenem and other beta-lactams in Klebsiella pneumoniae. *Antimicrob. Agents Chemother.*
432 **48**, 3203-3206, (2004).
433 6 Kaczmarek, F. M., Dib-Hajj, F., Shang, W. & Gootz, T. D. High-level carbapenem
434 resistance in a Klebsiella pneumoniae clinical isolate is due to the combination of bla(ACT-

1) beta-lactamase production, porin OmpK35/36 insertional inactivation, and down-regulation of the phosphate transport porin phoe. *Antimicrob. Agents Chemother.* **50**, 3396-3406, (2006).

7 Loli, A. *et al.* Sources of diversity of carbapenem resistance levels in Klebsiella pneumoniae carrying blaVIM-1. *The Journal of antimicrobial chemotherapy* **58**, 669-672, (2006).

8 Martinez-Martinez, L. *et al.* Activities of imipenem and cephalosporins against clonally related strains of Escherichia coli hyperproducing chromosomal beta-lactamase and showing altered porin profiles. *Antimicrob. Agents Chemother.* **44**, 2534-2536, (2000).

9 Mena, A. *et al.* Characterization of a large outbreak by CTX-M-1-producing Klebsiella pneumoniae and mechanisms leading to in vivo carbapenem resistance development. *J Clin Microbiol* **44**, 2831-2837, (2006).

10 Egger, L. A. & Inouye, M. Purification and characterization of the periplasmic domain of EnvZ osmosensor in Escherichia coli. *Biochem. Biophys. Res. Commun.* **231**, 68-72, (1997).

11 Forst, S. A. & Roberts, D. L. Signal transduction by the EnvZ-OmpR phosphotransfer system in bacteria. *Research in microbiology* **145**, 363-373, (1994).

12 Mizuno, T. His-Asp phosphotransfer signal transduction. *J Biochem* **123**, 555-563, (1998).

13 Hoch, J. A. & Silhavy, T. J. (American Society of Microbiology Press, Washington, DC, USA, 1995).

14 Gerken, H., Charlson, E. S., Cicirelli, E. M., Kenney, L. J. & Misra, R. MzrA: a novel modulator of the EnvZ/OmpR two-component regulon. *Mol Microbiol* **72**, 1408-1422, (2009).

15 Gerken, H. & Misra, R. MzrA-EnvZ interactions in the periplasm influence the EnvZ/OmpR two-component regulon. *J Bacteriol* **192**, 6271-6278, (2010).

16 Forst, S. A., Delgado, J. & Inouye, M. DNA-binding properties of the transcription activator (OmpR) for the upstream sequences of ompF in Escherichia coli are altered by envZ mutations and medium osmolarity. *J Bacteriol* **171**, 2949-2955, (1989).

17 Lan, C. Y. & Igo, M. M. Differential expression of the OmpF and OmpC porin proteins in Escherichia coli K-12 depends upon the level of active OmpR. *J Bacteriol* **180**, 171-174, (1998).

18 Russo, F. D. & Silhavy, T. J. EnvZ controls the concentration of phosphorylated OmpR to mediate osmoregulation of the porin genes. *J Mol Biol* **222**, 567-580, (1991).

19 Gushchin, I. *et al.* Mechanism of transmembrane signaling by sensor histidine kinases. *Science*, (2017).

20 Unnerstale, S., Maler, L. & Draheim, R. R. Structural characterization of AS1-membrane interactions from a subset of HAMP domains. *Biochim Biophys Acta* **1808**, 2403-2412, (2011).

21 Hulko, M. *et al.* The HAMP domain structure implies helix rotation in transmembrane signaling. *Cell* **126**, 929-940, (2006).

22 Zhou, Q., Ames, P. & Parkinson, J. S. Mutational analyses of HAMP helices suggest a dynamic bundle model of input-output signalling in chemoreceptors. *Mol Microbiol* **73**, 801-814, (2009).

23 Falke, J. J. & Hazelbauer, G. L. Transmembrane signaling in bacterial chemoreceptors. *Trends in biochemical sciences* **26**, 257-265, (2001).

24 Hazelbauer, G. L., Falke, J. J. & Parkinson, J. S. Bacterial chemoreceptors: high-performance signaling in networked arrays. *Trends in biochemical sciences* **33**, 9-19, (2008).

25 Parkinson, J. S., Hazelbauer, G. L. & Falke, J. J. Signaling and sensory adaptation in Escherichia coli chemoreceptors: 2015 update. *Trends in microbiology* **23**, 257-266, (2015).

26 Hwang, E. *et al.* Crystal structure of the EnvZ periplasmic domain with CHAPS. *FEBS Lett* **591**, 1419-1428, (2017).

27 Upadhyay, A. A., Fleetwood, A. D., Adebali, O., Finn, R. D. & Zhulin, I. B. Cache Domains That are Homologous to, but Different from PAS Domains Comprise the Largest Superfamily of Extracellular Sensors in Prokaryotes. *PLoS computational biology* **12**, e1004862, (2016).
28 Heininger, A., Yusuf, R., Lawrence, R. & Draheim, R. R. Identification of transmembrane helix 1 (TM1) surfaces important for EnvZ signalling and dimerisation. *Biochim. Biophys. Acta* **1858**, 1868-1875, (2016).
29 Hessa, T. *et al.* Molecular code for transmembrane-helix recognition by the Sec61 translocon. *Nature* **450**, 1026-1030, (2007).
30 Krogh, A., Larsson, B., von Heijne, G. & Sonnhammer, E. L. Predicting transmembrane protein topology with a hidden Markov model: application to complete genomes. *J Mol Biol* **305**, 567-580, (2001).
31 Bass, R. B., Butler, S. L., Chervitz, S. A., Gloor, S. L. & Falke, J. J. Use of site-directed cysteine and disulfide chemistry to probe protein structure and dynamics: applications to soluble and transmembrane receptors of bacterial chemotaxis. *Methods in enzymology* **423**, 25-51, (2007).
32 Draheim, R. R., Bormans, A. F., Lai, R. Z. & Manson, M. D. Tuning a bacterial chemoreceptor with protein-membrane interactions. *Biochemistry* **45**, 14655-14664, (2006).
33 Botelho, S. C., Enquist, K., von Heijne, G. & Draheim, R. R. Differential repositioning of the second transmembrane helices from E. coli Tar and EnvZ upon moving the flanking aromatic residues. *Biochim Biophys Acta* **1848**, 615-621, (2015).
34 Hall, B. A., Armitage, J. P. & Sansom, M. S. Transmembrane helix dynamics of bacterial chemoreceptors supports a piston model of signalling. *PLoS computational biology* **7**, e1002204, (2011).
35 Mise, T. Structural Analysis of the Ligand-Binding Domain of the Aspartate Receptor Tar from Escherichia coli. *Biochemistry* **55**, 3708-3713, (2016).
36 Norholm, M. H., von Heijne, G. & Draheim, R. R. Forcing the Issue: Aromatic Tuning Facilitates Stimulus-Independent Modulation of a Two-Component Signaling Circuit. *ACS Synth Biol* **4**, 474-481, (2015).
37 Batchelor, E. & Goulian, M. Robustness and the cycle of phosphorylation and dephosphorylation in a two-component regulatory system. *Proc Natl Acad Sci U S A* **100**, 691-696, (2003).
38 Miyashiro, T. & Goulian, M. High stimulus unmasks positive feedback in an autoregulated bacterial signaling circuit. *Proc Natl Acad Sci U S A* **105**, 17457-17462, (2008).
39 Siryaporn, A. & Goulian, M. Cross-talk suppression between the CpxA-CpxR and EnvZ-OmpR two-component systems in E. coli. *Mol Microbiol* **70**, 494-506, (2008).
40 Chervitz, S. A. & Falke, J. J. Molecular mechanism of transmembrane signaling by the aspartate receptor: a model. *Proc Natl Acad Sci U S A* **93**, 2545-2550, (1996).
41 Falke, J. J. Piston versus Scissors: Chemotaxis Receptors versus Sensor His-Kinase Receptors in Two-Component Signaling Pathways. *Structure* **22**, 1219-1220, (2014).
42 Molnar, K. S. *et al.* Cys-Scanning Disulfide Crosslinking and Bayesian Modeling Probe the Transmembrane Signaling Mechanism of the Histidine Kinase, PhoQ. *Structure* **22**, 1239-1251, (2014).
43 Cheung, J., Bingman, C. A., Reyngold, M., Hendrickson, W. A. & Waldburger, C. D. Crystal structure of a functional dimer of the PhoQ sensor domain. *J Biol Chem* **283**, 13762-13770, (2008).
44 Inouye, M. Signaling by transmembrane proteins shifts gears. *Cell* **126**, 829-831, (2006).
45 Norholm, M. H., von Heijne, G. & Draheim, R. R. 'Forcing the issue' - Aromatic tuning facilitates stimulus-independent modulation of a two-component signaling curcuit. *ACS Synth Biol*.

46 Casadaban, M. J. & Cohen, S. N. Analysis of gene control signals by DNA fusion and cloning in Escherichia coli. *J Mol Biol* **138**, 179-207, (1980).
47 Guyer, M. S., Reed, R. R., Steitz, J. A. & Low, K. B. Identification of a sex-factor-affinity site in E. coli as gamma delta. *Cold Spring Harb Symp Quant Biol* **45 Pt 1**, 135-140, (1981).
48 Batchelor, E., Silhavy, T. J. & Goulian, M. Continuous control in bacterial regulatory circuits. *J Bacteriol* **186**, 7618-7625, (2004).
49 Hsing, W. & Silhavy, T. J. Function of conserved histidine-243 in phosphatase activity of EnvZ, the sensor for porin osmoregulation in Escherichia coli. *J Bacteriol* **179**, 3729-3735, (1997).
50 Cantwell, B. J. *et al.* CheZ phosphatase localizes to chemoreceptor patches via CheA-short. *J Bacteriol* **185**, 2354-2361, (2003).
51 Southern, J. A., Young, D. F., Heaney, F., Baumgartner, W. K. & Randall, R. E. Identification of an epitope on the P and V proteins of simian virus 5 that distinguishes between two isolates with different biological characteristics. *The Journal of general virology* **72 (Pt 7)**, 1551-1557, (1991).
52 Miller, J. H. *A Short Course in Bacterial Genetics: A Laboratory Manual and Handbook for Escherichia coli and Related Bacteria*. (Cold Spring Harbor Laboratory Press, 1992).
53 Ausubel, F. M. *et al. Current Protocols in Molecular Biology*. (Wiley, 1998).
54 Schneider, C. A., Rasband, W. S. & Eliceiri, K. W. NIH Image to ImageJ: 25 years of image analysis. *Nat Methods* **9**, 671-675, (2012).
55 Van Der Spoel, D. *et al.* GROMACS: fast, flexible, and free. *Journal of computational chemistry* **26**, 1701-1718, (2005).

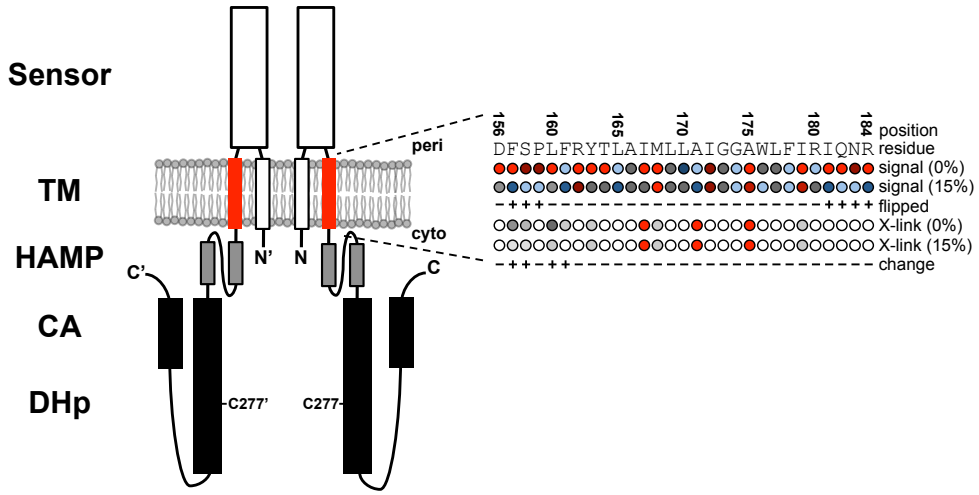
Sensor
TM
HAMP
CA
DHp
peri
cyto
N'
N
C'
C
C277'
C277
156
160
165
170
175
180
184
position
DFSPLFRYTLAIMLLAIGGAWLFIRIQNR
residue
signal (0%)
signal (15%)
flipped
X-link (0%)
X-link (15%)
change

Figure 1.

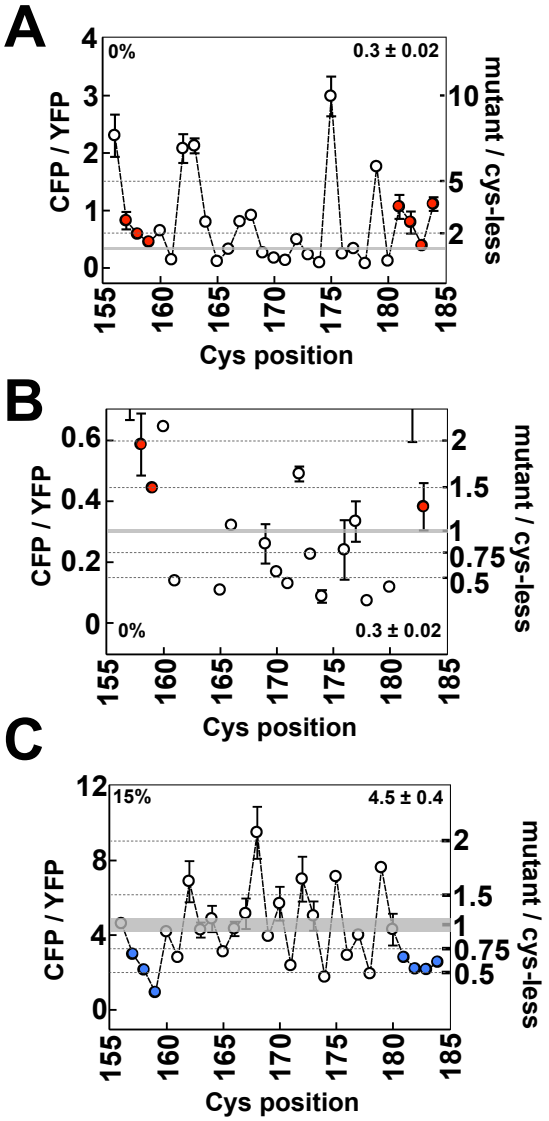
A
0%
0.3 ± 0.02
CFP / YFP
mutant / cys-less
Cys position
B
0%
0.3 ± 0.02
CFP / YFP
mutant / cys-less
Cys position
C
15%
4.5 ± 0.4
CFP / YFP
mutant / cys-less
Cys position

Figure 2.

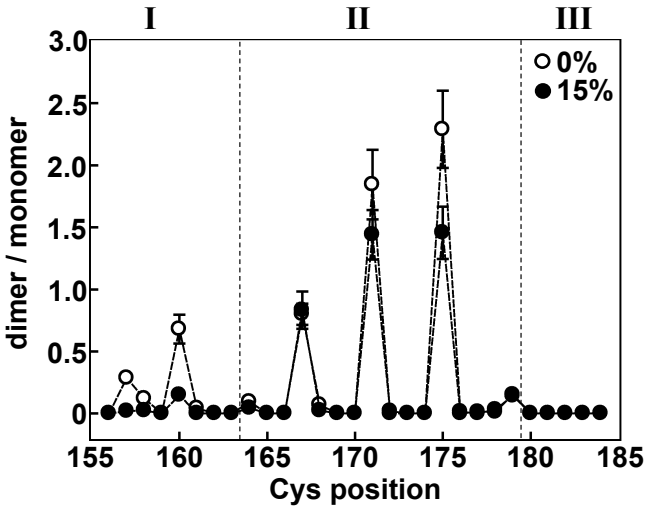
I
II
III
0%
15%
dimer / monomer
3.0
2.5
2.0
1.5
1.0
0.5
0
155
160
165
170
175
180
185
Cys position

Figure 3.

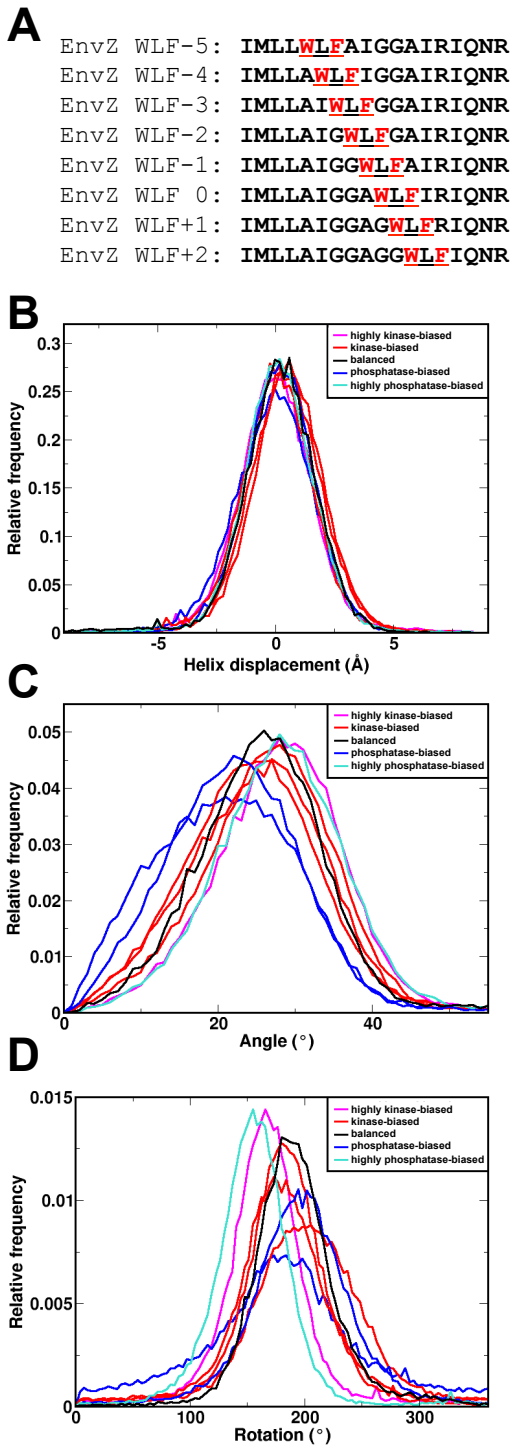
A
EnvZ WLF-5: IMLLWLFAIGGAIRIQNR
EnvZ WLF-4: IMLLAWLFIGGAIRIQNR
EnvZ WLF-3: IMLLAIWLFGGAIRIQNR
EnvZ WLF-2: IMLLAIGWLFGAIRIQNR
EnvZ WLF-1: IMLLAIGGWLFAIRIQNR
EnvZ WLF 0: IMLLAIGGAWLFIRIQNR
EnvZ WLF+1: IMLLAIGGAGWLFRIQNR
EnvZ WLF+2: IMLLAIGGAGGWLFIQNR
B
highly kinase-biased
kinase-biased
balanced
phosphatase-biased
highly phosphatase-biased
Relative frequency
Helix displacement (Å)
C
Angle (°)
D
Rotation (°)

Figure 4.